PHYSICAL REVIEW B **94**, 075431 (2016)

Structure and magnetism of the (2 × 2)-FeO(111) surface

I. Bernal-Villamil and S. Gallego[*]
Instituto de Ciencia de Materiales de Madrid, Consejo Superior de Investigaciones Científicas, Cantoblanco, 28049 Madrid, Spain

(Received 25 May 2016; revised manuscript received 18 July 2016; published 23 August 2016)

Based on *ab initio* calculations, we determine the features and relative stability of different models proposed to describe the (2 × 2)-FeO(111) reconstruction. Our results suggest that both wurtzite and spinel-like environments are possible, and their coexistence explains phenomena of biphase ordering. The surface phase diagram reflects a competition of charge and magnetic compensation effects, and reveals the important influence of the substrate on the final surface structure. Though antiferromagnetic couplings are dominant, frustration and the delicate balance of surface and bulk exchange interactions lead to a net surface magnetization that accounts for the large measured values.

DOI: 10.1103/PhysRevB.94.075431

I. INTRODUCTION

The surfaces of binary Fe oxides are at the forefront of advanced technologies. Because of their biocompatibility, they occupy a unique position in nanomagnetism, with applications in areas as diverse as spintronics and biomedicine [1,2]. But they are also important due to their catalytic activity, in the design of gas sensor devices and for hydrogen storage [3–5], which confers increasing interest in the detailed knowledge of their structural and electronic properties under different environments. Among these surfaces, those of FeO have an additional interest in the design of exchange-bias nanocomposites [6,7]. Particularly, the FeO(111) termination is a good candidate to achieve large perpendicular magnetic anisotropy [8] and has already been used as support of hexagonal two-dimensional materials such as graphene [9].

Previous studies of the FeO(111) surface have led to a considerable dispersion of results, partly due to the difficulties to prepare high-quality samples. On one hand, the bulk form only exists at ambient conditions with a significant 5–15% of Fe vacancies, and these vacancies tend to organize in different arrangements of local spinel-like clusters [10]. Though $Fe_{1-x}O$ samples can be stabilized by fast quenching, it is difficult to discern these clusters from Fe_3O_4 inclusions, which complicates their characterization. On the other hand, the phase diagram of binary Fe oxides can be strongly altered under reduced dimensions. As a result, the preparation conditions in epitaxial growth are crucial to achieve phase selectivity [11–13]. In particular, while bulk FeO spontaneously decomposes into Fe_3O_4 and Fe, a precursor FeO layer forms during growth of $Fe_3O_4(111)$ on most substrates, and often remains at the substrate/Fe_3O_4 interface [14]. Also at the $Fe_3O_4(111)$ surface, a two-dimensional superlattice of Fe_3O_4 and FeO islands forms under low oxygen pressures (*biphase ordering*), which under further reduction transforms to only FeO islands covering the Fe_3O_4 substrate [15].

The tendency of stoichiometric FeO(111) to become stable in the ultrathin limit has been evidenced in numerous studies of mono- and bilayer FeO(111) films on different supports. Most works have been performed on Pt(111) [16–18], but the use of other metals and substrate orientations, including Pt(100) [16], Pd(111) [19], Pd(100) [20], Ag(111) [21], Ag(100) [22,23], Cu(110) [24], or Ru(0001) [25], and even of different oxides such as YSZ(001) [26] or α-$Al_2O_3(0001)$ [27], has been reported. Though the substrate introduces subtle variations that manifest, for example, in the reactivity of the ultrathin film, in all cases the Fe oxide seems to adopt an O-ended surface and a structure similar to the bulk, with a slightly expanded in-plane lattice and dominant antiferromagnetic order [28,29]. Different attempts have been performed to overcome the bilayer-thickness limit and grow thicker FeO films [21,24,30,31]. The record thickness corresponds to 8-nm-thick high-quality, stoichiometric FeO films with bulklike properties obtained under reducing conditions on Ru(0001) [32]. These films show a (1 × 1) O termination that requires a wurtzite (WZ) stacking at the outermost surface layers, while preserving the AF-II magnetic order of FeO (namely, ferromagnetic Fe planes with opposite spin orientation in alternation along the [111] axis).

But even though a (1 × 1) pattern has been found at slightly thinner FeO films on different substrates [23,33], reconstructions emerge at higher O pressures: a $\sqrt{3} \times \sqrt{3}R30^\circ$ surface linked to a transformation to α-$Fe_2O_3(0001)$ [34], and a poorly understood (2 × 2) structure [11,35–37]. Different possibilities have been proposed to explain the (2 × 2) symmetry, including stacking faults, an octopolar termination, or the initial transformation to spinel $Fe_3O_4(111)$, but its actual origin remains unclear. The Fe valence is used to discriminate between FeO (with only Fe^{2+}) and Fe_3O_4 (with also Fe^{3+}), but we have recently shown that Fe^{3+} states may emerge even at the ideal rock-salt (RS) bulk truncation [32]. As a further complication, sometimes the (2 × 2) symmetry corresponds to an actual transformation of the entire film to Fe_3O_4 [38]. At present, there is no information about the electronic features of the spinel or octopolar geometries at the surface of a FeO(111) film. More intriguing, for thin enough films grown on Fe(110), the (2 × 2) pattern can be accompanied by the emergence of ferromagnetism of high magnetization and ordering temperature [36], tentatively explained assuming a model with significant Fe excess at the surface [see Fig. 1(b)]. But such model is contrary to the common evidence of an O-rich termination and to the fact that FeO is the end phase in the Fe-rich limit. Studies on nanoscaled films of FeO(111) have also measured a net magnetization that may survive at high temperatures, but the magnetism seems to be linked to

---

[*] sgallego@icmm.csic.es

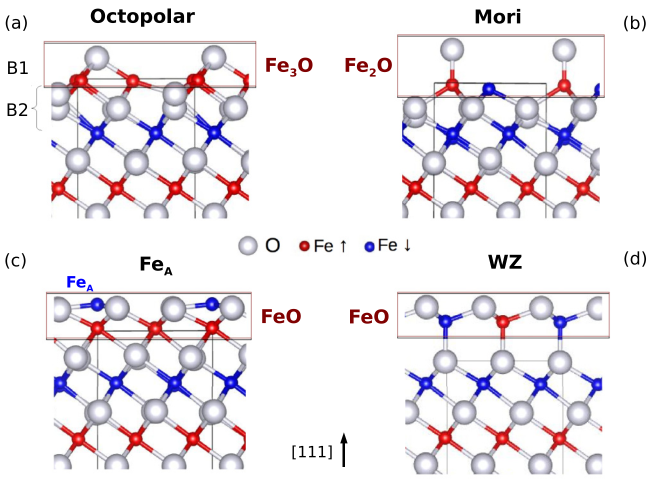

FIG. 1. Side view of the surface models considered, represented under their most stable structural and magnetic configurations, and indicating the stoichiometry of the squared region B1 (see text for details). The gray lines in the back are a guide to delimit the size of the (2 × 2) unit cell.

buried nanostructures or interface effects, with no contribution from the bare surface [30,39,40].

In the present work, we address the detailed investigation of the (2 × 2)-FeO(111) surface based on *ab initio* calculations that continue our previous study of the unreconstructed termination [32]. Our purpose is to determine the accuracy of the models proposed from the experiments to describe the (2 × 2) reconstruction, based both on their relative stability and their ability to reproduce the measured properties. Moreover, as we will show, our results account for the existence of biphase ordering phenomena.

II. METHODS

The conditions of the calculations have been explained elsewhere [32]. We use the density functional theory as implemented in the VASP code [41], based on the projector augmented wave (PAW) method to consider the core electrons. The exchange-correlation part is described with the Perdew-Burke-Ernzerhof parametrization of the generalized gradient approximation modified for solids (PBEsol), including an effective local $U - J$ term following the Dudarev approach. The value $U - J = 4$ eV has been chosen after calculations of bulk FeO [10].

We have modeled O-ended (2 × 2)-FeO(111) slabs with the RS lattice of bulk FeO and a thickness of 9–10 planes, supported on a Ru(0001) layer and including a vacuum region of 14 Å. For all models and magnetic couplings, the atomic positions of the five outermost surface layers have been fully relaxed using a 5 × 5 × 1 Monkhorst-Pack sampling of the Brillouin zone until the forces on the atoms were below 0.01 eV Å^{-1}. Convergence in the electronic properties and relative stabilities were then obtained with $9 \times 9 \times 2\,k$ samplings.

Figure 1 shows the different surface models considered by us. The surface region comprised of the four outermost planes includes a subsurface O-Fe bilayer (labeled B2) that resembles the bulk, and a surface O-Fe bilayer (B1, squared in the figure) that contains all relevant modifications. Besides the models in the figure, we have also explored the possibility of a local hcp stacking at B1, as proposed from analysis of low-energy electron diffraction (LEED) beam profiles [37]. Such stacking increases the energy over the ideal RS termination over 1 eV. A WZ sequence would also provide only two types of stacking sites at the surface region comprised by B1+B2, and can be at the origin of the results in Ref. [37].

Both the octopolar [42] and Mori [36] structures are based on partial removal of O atoms at B1, resulting in surface stoichiometries with an unlikely Fe excess. The Fe_A model departs from the natural evolution of the rock-salt FeO(111) stacking to a spinel $Fe_3O_4(111)$ structure, shifting one Fe cation from the outermost Fe layer to a tetrahedral coordination site (Fe_A) above the surface O plane. It also represents locally the surface environment corresponding to a 4:1 cluster of Fe vacancies [10]. As evidenced in the figure, the position of this Fe_A cation relaxes to become almost coplanar to O, and the 1:1 Fe:O ratio is preserved at B1. Finally, we have considered a WZ termination [32] where the (2 × 2) symmetry is introduced by the presence of in-plane antiferromagnetic couplings. The electronic properties of the (1 × 1) WZ surface were already detailed in Ref. [32], and they are not significantly modified by the introduction of in-plane antiferromagnetism at B1. Except for this WZ model, bulk electronic features are essentially recovered at B2 in all cases.

III. MAGNETIC CONFIGURATIONS

For these structural models, we have explored all possible collinear magnetic couplings between Fe atoms at B1 and B2 compatible with the (2 × 2) symmetry, while keeping the AF-II order at the layers below. Extending modifications of the AF-II order beyond B2 increased the total energy of the system. A weak noncollinear magnetic component has been reported at the FeO(100) surface [8], but it emerges from the competition between the surface magnetic easy axis—that favors a perpendicular (to the surface) magnetization—and the bulk one—that lies along the (111) direction. Such competition is not expected at the (111) surface, where a perpendicular magnetic component would align with the bulk easy axis. Furthermore, while evidence of noncollinear magnetic order has been found at bulk CoO, the opposite holds for FeO [43], justifying our approach.

The representative inequivalent configurations are shown in Fig. 2. Though each configuration was allowed to relax independently, their structural differences for a fixed surface model are minor, and do not alter the trends of relative stabilities. It is important to keep in mind that we are dealing with a magnetically frustrated system close to a charge instability, which under certain conditions may not even converge to a stable ground state (e.g., full ferromagnetism at B1 and B2). Though under this situation we cannot provide a quantitative energy barrier, this indicates that the explored solution is not favorable for the system.

The most stable magnetic solutions are those represented in Fig. 1. In the particular case of the Mori model, we found as the stable magnetic order the same as that proposed from the experiments, i.e., the AF-surf configuration of Fig. 2, which lowers the energy with respect to the AF-II and

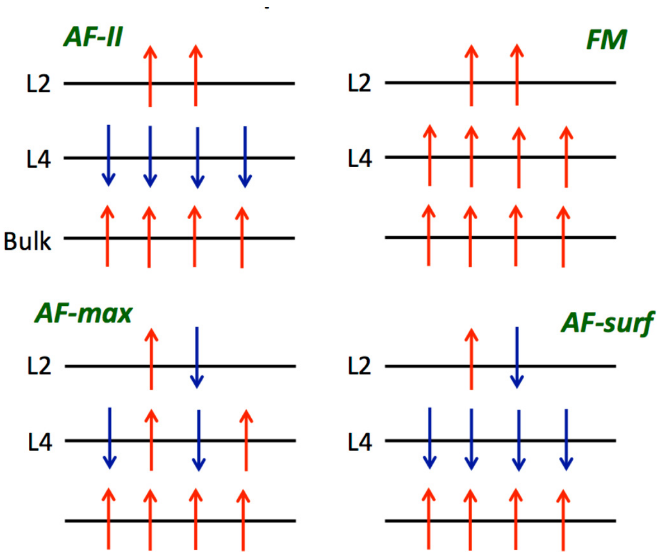

FIG. 2. Schematic representation of the different types of magnetic coupling considered for Fe atoms at B1 and B2.

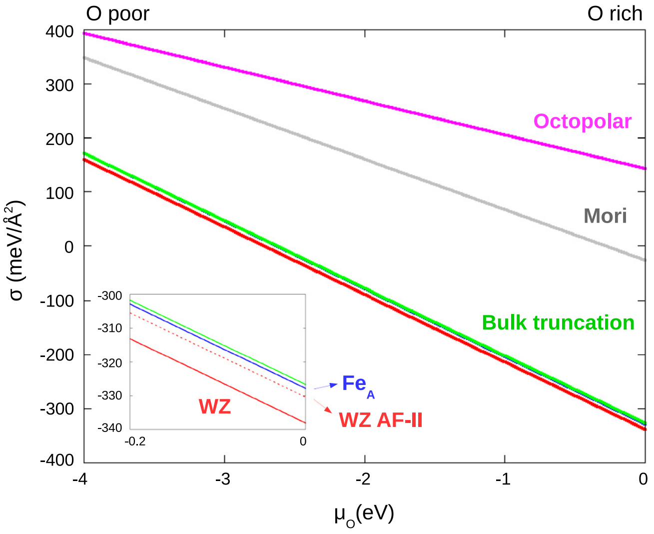

FIG. 3. Surface energy (σ) of the models in Fig. 1 as a function of the O chemical potential (μ_O). The RS (bulk truncation) and WZ terminations under AF-II order are also shown. The inset is a zoom of the lower right corner of the graph.

AF-max couplings by 260 and 140 meV, respectively. An analysis of all of our results allows us to extract the following conclusions: (i) shifting the AF-II order beyond B1 is always unfavorable, and (ii) antiferromagnetic couplings dominate at the surface region, but the balance of in-plane and interlayer exchange interactions at B1 and B2 depends on the detailed surface geometry and composition. The result is the continuity of the AF-II order under the octopolar and Fe_A terminations, while in-plane antiferromagnetism sets in at B1 for the rest of the cases. We would like to remark that we found such in-plane order to be favorable also under a RS surface termination, but the surface WZ stacking continues to be preferred over the RS one.

IV. RESULTS AND DISCUSSION

Once we have the ground-state magnetic configurations, we can determine the relative stability of the different surface models. The identical stoichiometry of the Fe_A and WZ structures allows direct comparison of their total energies. However, consideration of the Mori and octopolar geometries requires one to take into account variations of the chemical potentials. In order to do so, the surface energy (σ) of all models has been computed following standard thermodynamic approximations [32,44]. Since we have constructed asymmetric slabs supported on Ru and we are interested only in the O-ended surface, we refer the total energies to the common quantity $N_{Ru}\mu_{Ru}$, with μ_{Ru} extracted from the total energy of bulk Ru [45]. The results are shown in Fig. 3, where the lowest surface energy corresponds to the most stable situation. As a reference, the AF-II solutions for the RS bulk truncation and the WZ termination are also shown. It is evident that, as occurred at the unreconstructed surface, the WZ stacking is always favored. Also, the Mori and octopolar models can be discarded even in the O-poor limit. On the other hand, the Fe_A solution is close in energy to the bulk truncation and the WZ model, particularly when all are kept under a common AF-II magnetic order. These reduced energy differences explain the ease to transform the FeO(111) structure to a spinel-like surface, and the emergence of biphase ordering.

To better understand this surface phase diagram, we explore in detail the properties of the FeO(111) reconstruction inherent to the different models. An important aspect to take into account regarding the stabilization of the surface is the ability to compensate the loss of donor charge due to O bond breaking. Table I shows the mean Bader charges of the O and Fe atoms at B1 for all cases. From the values for O, it is evident that the Mori model leaves a high-O charge deficiency, making it quite implausible. The most efficient charge compensation is provided by the octopolar geometry, while the rest of the situations represent a slight improvement over the ideal bulk truncation. But the large surface energy of the octopolar solution suggests that effects beyond mere charge compensation must influence the actual (2 × 2)-FeO(111) structure. Regarding the Fe charge, it contains information about the valence state of the surface Fe atoms [10,32]: values above 6.5 are linked to Fe^{2+}, typical of FeO, while lower values represent a change to Fe^{3+}. From the table, Fe^{3+} only exists at the Fe_A model, and not only at the tetrahedral Fe_A site, but

TABLE I. Mean Bader charge (Q) of the O and Fe atoms at B1, and net magnetization (in μ_B per unit cell) at both B1 (M_{B1}) and the entire surface region (M_{B1+B2}) for the structures in Fig. 1. Corresponding values for the ideal AF-II RS bulk truncation are also shown. In the Fe_A model, the Q(Fe) value of the Fe_A atom is distinguished from the rest.

Model	Q(O)	Q(Fe)	M_{B1}	M_{B1+B2}
Octopolar	7.18	6.79	11.3	3.3
Mori	6.80	6.67	0.8	15.0
Fe_A	7.08	$6.48_A/6.31$	9.3	5.1
WZ	7.09	6.55	0.3	15.7
Bulk truncation	7.06	6.31	18.7	4.4

at the entire B1 bilayer. This serves to discard proposals of an octopolar geometry for FeO films grown on Pt(111), where Fe^{3+} states have been measured [34]. On the other hand, only Fe^{2+} contributions have been identified at ultrathin films grown on Fe(110) [35], which would be compatible with all models except Fe_A. Thus, analysis of the surface charge supports that the (2 × 2)-FeO(111) surface admits multiple solutions, in good agreement with the relative stabilities in Fig. 3. Furthermore, it reveals a substantial influence of the substrate on the surface phase diagram, opposite to the unreconstructed termination.

Further insights can be obtained from the surface magnetization arising from the different models. Previously we showed that antiferromagnetic interactions dominate at the outermost layers. However, this does not necessarily imply the lack of a net surface magnetization. This is best understood regarding the rightmost columns of Table I, where we have compiled the sum of individual atomic magnetic moments at both B1 and the entire surface region (B1+B2) for the stable magnetic solutions in Fig. 1. Even without any reconstruction, creation of the surface causes an uncompensated magnetization [32], reflected in the data for the bulk truncation. Its value is enlarged by the slight enhancement of the Fe magnetic moments at the surface layer, and also by the increased magnetization induced in the outermost O atoms, which are only bonded to Fe atoms with one spin orientation. These effects are also present under the (2 × 2) reconstruction, though depending on the surface structure, the individual Fe contributions at B1 may or may not sum up. For cases that preserve the AF-II order, the magnetization at B1 is large, and even after adding the contribution from B2 it remains significant, with the largest value for the Fe_A case. Oppositely, when in-plane antiferromagnetism exists, as occurs for the Mori and WZ models, the magnetization at B1 is almost negligible, while the sum of B1 and B2 is very large. Interestingly, the maximum value does not correspond to the Mori solution, but to the more stable WZ termination. In summary, both the WZ and Fe_A structures can explain the existence of a large magnetization at the surface that surpasses that of a simple bulk truncation. Though our calculations do not address the estimation of the magnetic ordering temperature, the moderate magnetic energy differences suggest that the high measured values arise from substrate-induced effects in the ultrathin limit, as also pointed out from the experimental evidence [36].

V. CONCLUSIONS

We conclude that the (2 × 2) FeO(111) surface is a manifestation of different surface structures, whose relative stability is largely conditioned by the choice of the substrate and the preparation conditions. On one hand, it may be due to a local spinel structure, which either allocates Fe defect clusters or initiates a transition to $Fe_3O_4(111)$. On the other hand, it may hold a WZ termination similarly to the unreconstructed surface. Both structures are based on the introduction of local tetrahedral environments at the outermost layers, but can be distinguished by their distinct signatures concerning the presence of Fe^{3+} states and the distribution of magnetic moments. The coexistence of both solutions within a narrow energy window explains the origin of biphase ordering, and makes room for the large influence of the substrate on the final structure.

The surface phase diagram obtained here reveals a subtle and complex role of magnetic interactions, a situation similar to that found in bulk FeO [10]. While our results clearly discard a ferromagnetic solution, magnetic noncompensation gives rise to large values of the surface magnetization. A further complication that deserves to be considered is the influence of the distribution of Fe vacancies at the inner oxide layers, which could alter the surface magnetic properties. However, for the ultrathin films where the (2 × 2)-FeO(111) symmetry has been measured, good stoichiometry at the inner layers can be assumed. As a final consideration, in principle, the surface magnetization reported here should be distinguished from the magnetization measured at ultrathin FeO(111) films of 1–2 nm thickness [30], more likely arising from the evolution of the in-plane antiferromagnetism of the monolayer towards the layered bulklike AF-II order. However, a nonzero surface contribution may exist, and should be taken into account to explain the complex spectral magnetic features.

Our work represents a first step towards the understanding of the FeO(111) surface phase diagram. It serves to rationalize the interpretation of the experiments, providing a reference to identify intrinsic contributions arising from a defect-free FeO film. This can be used as the starting point of an ambitious molecular dynamics study directly incorporating substrate and temperature effects. The complete picture still remains a challenging task, complicated by the ease to trigger the mutual transformation between the different binary Fe oxide phases at the nanoscale, largely conditioned by both external parameters (such as the choice of the substrate or the preparation conditions) and the presence of intrinsic defects or disorder.

ACKNOWLEDGMENTS

This research was supported by the Spanish Ministry of Economy and Competitiveness (MINECO) through Grant No. MAT2012-38045-C04-04. I.B. acknowledges CSIC for the JAE program. The VESTA package [46] has been used to create some of the original figures of this paper.

---

[1] A. Lin, J. Rodrigues, C. Su, M. Milletari, K. Loh, T. Wu, W. Chen, A. Castro Neto, A. Adam, and S. Wee, Sci. Rep. **5**, 11430 (2015).
[2] P. Tartaj, M. Morales, T. González-Carreño, S. Veintemillas-Verdaguer, and C. Serna, Adv. Mater. **23**, 5243 (2011).
[3] H.-J. Freund, Surf. Sci. **601**, 1438 (2007).
[4] N. Viet Long, T. Teranishi, Y. Yang, C. Thi, Y. Cao, and M. Nogami, Int. J. Metallurg. Mater. Eng. **1**, 119 (2015).
[5] K. Otsuka, C. Yamada, T. Kaburagi, and S. Takenaka, Int. J. Hydrogen Energ. **28**, 335 (2003).

[6] V. Skumryev, S. Stoyanov, Y. Zhang, G. Hadjipanayis, D. Givord, and J. Nogués, Nature (London) **423**, 850 (2003).
[7] X. Sun, N. Frey Huis, A. Sigdel, and S. Sun, Nano Lett. **12**, 246 (2012).
[8] A. Schrön and F. Bechstedt, Phys. Rev. B **92**, 165112 (2015).
[9] A. Dahal and M. Batzill, Sci. Rep. **5**, 11378 (2015).
[10] I. Bernal-Villamil and S. Gallego, Phys. Rev. B **90**, 195126 (2014).
[11] Y. Gao, Y. Kim, and S. A. Chambers, J. Mater. Res. **13**, 2003 (1998).
[12] G. Ketteler and W. Ranke, J. Phys. Chem. B **107**, 4320 (2003).
[13] M. Monti, B. Santos, A. Mascaraque, O. Rodríguez de la Fuente, M. Niño, T. O. Mentes, A. Locatelli, K. McCarty, J. Marco, and J. de la Figuera, J. Phys. Chem. C **116**, 11539 (2012).
[14] I. Bernal-Villamil and S. Gallego, J. Phys.: Condens. Matter **27**, 012001 (2015).
[15] N. G. Condon, F. M. Leibsle, T. Parker, A. R. Lennie, D. J. Vaughan, and G. Thornton, Phys. Rev. B **55**, 15885 (1997).
[16] G. Vurens, V. Maurice, M. Salmeron, and G. Somorjai, Surf. Sci. **268**, 170 (1992).
[17] T. Schedel-Niedrig, W. Weiss, and R. Schlögl, Phys. Rev. B **52**, 17449 (1995).
[18] Y. J. Kim, C. Westphal, R. X. Ynzunza, H. C. Galloway, M. Salmeron, M. A. Van Hove, and C. S. Fadley, Phys. Rev. B **55**, R13448(R) (1997).
[19] H. Zeuthen, W. Kudernatsch, G. Peng, L. Merte, L. Ono, L. Lammich, Y. Bai, L. Grabow, M. Mavrikakis, S. Wendt, and F. Besenbacher, J. Phys. Chem. C **117**, 15155 (2013).
[20] D. Kuhness, S. Pomp, V. Mankad, G. Barcaro, L. Sementa, A. Fortunelli, F. Netzer, and S. Surnev, Surf. Sci. **69**, 133 (2016).
[21] G. Waddill and O. Ozturk, Surf. Sci. **575**, 35 (2005).
[22] D. Bruns, I. Kiesel, S. Jentsch, S. Lindemann, C. Otte, T. Schemme, T. Kuschel, and J. Wollschläger, J. Phys.: Condens. Matter **26**, 315001 (2014).
[23] L. Merte, M. Shipilin, S. Ataran, S. Blomberg, C. Zhang, A. Mikkelsen, J. Gustafson, and E. Lundgren, J. Phys. Chem. C **119**, 2572 (2015).
[24] E. Yagasaki and K. Kishi, J. Electron Spectrosc. Relat. Phenom. **69**, 133 (1994).
[25] I. Palacio, M. Monti, J. F. Marco, K. F. McCarty, and J. d. l. Figuera, J. Phys.: Condens. Matter **25**, 484001 (2013).
[26] I. Ermanoski and G. Kellogg, Surf. Sci. **614**, 1 (2013).
[27] S. Gota, E. Guiot, M. Henriot, and M. Gautier-Soyer, Surf. Sci. **454-456**, 796 (2000).
[28] L. Giordano, G. Pacchioni, J. Goniakowski, N. Nilius, E. D. L. Rienks, and H. J. Freund, Phys. Rev. B **76**, 075416 (2007).
[29] W. Zhang, Z. Li, Y. Luo, and J. Yang, J. Phys. Chem. C **113**, 8302 (2009).
[30] N. Spiridis, D. Wilgocka-Slezak, K. Freindl, B. Figarska, T. Giela, E. Mlynczak, B. Strzelczyk, M. Zajac, and J. Korecki, Phys. Rev. B **85**, 075436 (2012).
[31] J. Corneille, J.-W. He, and D. Goodman, Surf. Sci. **338**, 211 (1995).
[32] L. Martín-García, I. Bernal-Villamil, M. Oujja, E. Carrasco, R. Gargallo-Caballero, M. Castillejo, J. Marco, S. Gallego, and J. de la Figuera, J. Mater. Chem. C **4**, 1850 (2016).
[33] S. Liu, S. Wang, J. Guo, and Q. Guo, RSC Adv. **2**, 9938 (2012).
[34] H. Galloway, J. Benítez, and M. Salmeron, J. Vac. Sci. Technol. A **12**, 2302 (1994).
[35] D. Cappus, M. Hassel, E. Neuhaus, M. Heber, F. Rohr, and H.-J. Freund, Surf. Sci. **337**, 268 (1995).
[36] K. Mori, M. Yamazaki, T. Hiraki, H. Matsuyama, and K. Koike, Phys. Rev. B **72**, 014418 (2005).
[37] W. Weiss and G. Somorjai, J. Vac. Sci. Technol. A **11**, 2138 (1993).
[38] H.-J. Kim, J.-H. Park, and E. Vescovo, Phys. Rev. B **61**, 15284 (2000).
[39] G. S. D. Beach, F. T. Parker, D. J. Smith, P. A. Crozier, and A. E. Berkowitz, Phys. Rev. Lett. **91**, 267201 (2003).
[40] S. Couet, K. Schlage, R. Rüffer, S. Stankov, T. Diederich, B. Laenens, and R. Röhlsberger, Phys. Rev. Lett. **103**, 097201 (2009).
[41] G. Kresse and J. Furthmüller, Phys. Rev. B **54**, 11169 (1996).
[42] D. Wolf, Phys. Rev. Lett. **68**, 3315 (1992).
[43] K. Tomiyasu, T. Inami, and N. Ikeda, Phys. Rev. B **70**, 184411 (2004).
[44] K. Reuter and M. Scheffler, Phys. Rev. B **65**, 035406 (2001).
[45] C. Franchini, V. Bayer, R. Podloucky, G. Parteder, S. Surnev, and F. P. Netzer, Phys. Rev. B **73**, 155402 (2006).
[46] K. Momma and F. Izumi, J. Appl. Crystallogr. **44**, 1272 (2011).